Genetically targeted reporter imaging of deep neuronal network in the mammalian brain

Masafumi Shimojo[1,*], Maiko Ono[1], Hiroyuki Takuwa[1], Koki Mimura[1], Yuji Nagai[1], Masayuki Fujinaga[2], Tatsuya Kikuchi[2], Maki Okada[2], Chie Seki[1], Masaki Tokunaga[1], Jun Maeda[1], Yuhei Takado[1], Manami Takahashi[1], Takeharu Minamihisamatsu[1], Ming-Rong Zhang[2], Yutaka Tomita[3], Norihiro Suzuki[3], Anton Maximov[4], Tetsuya Suhara[1], Takafumi Minamimoto[1], Naruhiko Sahara[1], Makoto Higuchi[1,*]

Affiliations:

[1]Department of Functional Brain Imaging Research, National Institutes for Quantum and Radiological Science and Technology, Chiba, Japan

[2]Department of Radiopharmaceuticals Development, National Institutes for Quantum and Radiological Science and Technology, Chiba, Japan

[3]Department of Neurology, Keio University School of Medicine, Tokyo, Japan

[4]Department of Neuroscience, The Scripps Research Institute, La Jolla, CA, USA

*Correspondence to: shimojo.masafumi@qst.go.jp (M.S.); higuchi.makoto@qst.go.jp (M.H.)

Abstract:
Positron Emission Tomography (PET) allows biomolecular tracking, while PET monitoring of brain networks has been hampered by the lack of a suitable reporter. Here, we describe *in-vivo* brain reporters utilizing bacterial dihydrofolate reductase, ecDHFR, and its antagonist, TMP. In mice, peripheral administration of radiofluorinated and fluorescent TMP analogs enabled PET and intravital microscopy, respectively, of neuronal ecDHFR expressions. This technique was applicable to the visualization of chemogenetically provoked neuronal ensemble activities in the hippocampus. Notably, ecDHFR-PET captured neuronal projections in non-human primate brains, indicating the availability of ecDHFR-based techniques for network monitoring. Finally, we demonstrated PET assays of turnover and self-assembly of proteins tagged with ecDHFR mutants. Collectively, the current reporter technology offers diverse *in-vivo* molecular analyses of a brain circuit.

Main Text

Contemporary methods for live imaging of genetically-encoded reporters have transformed basic and translational neuroscience (*1, 2*). Many excellent fluorescence tools have recently been introduced for the visualization of neuronal ensembles and individual synapses, and for understanding the roles of neuronal cells in circuit development, function, and dysfunction (*3-5*). Despite its tremendous utility, fluorescence imaging remains largely unsuitable for simultaneous non-invasive monitoring of reporters in deep brain regions or across the entire brain because of light scattering and relatively narrow fields of view. One promising strategy for solving this technical bottleneck is to complement optical microscopy with positron emission tomography (PET). While PET itself has a limited spatiotemporal resolution, a combination of the two techniques may offer comprehensive insights into the dynamics of molecules of interest on scales ranging from subcellular to global levels (*6*). The major challenge for such a bimodal analysis of exogenous markers genetically targeted in the brain is the development of selective radioactive ligands that efficiently penetrate the blood-brain barrier (BBB) (*7*). A recent study reported brain PET imaging with an isoform of pyruvate kinase, PKM2, and its associated radiotracer [^{18}F]DASA-23 (*8*). Our laboratory has also demonstrated that a designer receptor exclusively activated by designer drugs (DREADD) and its artificial ligands, such as clozapine-N-oxide (CNO) and deschloroclozapine (DCZ), labeled with ^{11}C could be employed for PET of neurons and transplanted iPS cells in animal brains (*9-11*). Nonetheless, these compounds cannot be applied to bimodal imaging, and they may also suffer from undesired effects on endogenous substrates (*8, 12*).

E. coli dihydrofolate reductase (ecDHFR) is an enzyme whose activity is specifically blocked by a small antibiotic, trimethoprim (TMP). TMP rapidly diffuses through tissues, passes the BBB, and, importantly, lacks native targets in mammals (*13*). Moreover, TMP can be conjugated with fluorophores, and its radioactive analog, [^{11}C]TMP, is compatible with PET (*14, 15*). We hypothesized that ecDHFR, along with TMP, could be a suitable candidate for bimodal optical and PET imaging of the neuronal circuits and their function in intact brains (**Fig. 1A**). To explore this possibility, we first examined the utility of a red fluorophore-conjugated TMP derivative, TMP-hexachlorofluorescein (TMP-HEX), as a probe for optical imaging of ecDHFR in the brains of living mice. We locally introduced ecDHFR-EGFP into the mouse somatosensory cortex by an adeno-associated virus (AAV) vector under control of a pan-neuronal synapsin promoter (**Figs. S1A and S1C**). Awake

animals were examined by intravital two-photon laser microscopy after a single bolus tail vein administration of TMP-HEX. Individual neurons carrying ecDHFR-EGFP retained TMP-HEX, indicating that the compound penetrates the BBB similarly to conventional TMP (**Fig. 1B**). Importantly, intraperitoneal administration of a saturating dose of unlabeled TMP prior to the imaging session almost completely blocked the binding of TMP-HEX to ecDHFR, supporting the specificity of TMP-HEX for ecDHFR *in vivo* (**Figs. 1B and 1C**).

To accomplish an *in vivo* macroscopic analysis of ecDHFR distribution in the brain by PET, [^{18}F]fluoroethoxy-TMP ([^{18}F]FE-TMP), a high-affinity ^{18}F-labeled TMP derivative that has a prolonged half-life in radioactivity compared to conventional [^{11}C]TMP (**Figs. S3 and 1D**), was next synthesized and injected into the tail vein of mice expressing ecDHFR-EGFP or red fluorescent protein, mCherry, as a control, followed by dynamic PET scans. Remarkably, mice expressing ecDHFR-EGFP exhibited strong radiosignals on an ipsilateral side of the somatosensory cortex locally delivered with AAV encoding ecDHFR-EGFP, but not in uninfected areas of the contralateral side or ipsilateral side expressing mCherry (**Fig. 1E and 1F**). Pre-administration of unlabeled TMP significantly attenuated the enriched radioactive signals of [^{18}F]FE-TMP on the ipsilateral side expressing ecDHFR-EGFP **(Fig. 1G)**, indicating saturable and specific binding of [^{18}F]FE-TMP to ecDHFR. Taken together, these results demonstrate that TMP analogs can be used for multiscale optical and PET imaging of ecDHFR-based reporters in the brains of live animals.

To take advantage of the advanced utility of ecDHFR reporter for PET monitoring of neural circuit activations, we incorporated robust activity marking (RAM) system, an optimized synthetic activity-regulated element with the immediate early gene (IEG) cFos minimal promoter, which can drive the expression of a reporter protein in response to sensory stimuli and epileptic seizure (*16*) (**Fig. 2A**). RAM-dependent efficient marking of neuronal activation was successfully validated in cultured neurons (**Fig. S7A**). We then co-introduced AAVs encoding ecDHFR-d2Venus with RAM promoter and the excitatory DREADD, hM3Dq, into one side of the somatosensory cortex and examined the time-course change of the reporter expression by two-photon laser microscopy after air-puff stimulation of whiskers or hM3Dq activation via an intraperitoneal bolus administration of CNO. Repetitive sensory inputs by air-puff stimulation of whiskers robustly enhanced the fluorescence signals of ecDHFR-d2Venus in neurons, whereas the activation of hM3Dq more prominently induced signal enhancement in neurons expressing ecDHFR-d2Venus at 24 h after systemic administration of CNO (**Figs. 2B and 2C**). We then prepared mice co-expressing RAM-

ecDHFR-d2Venus and hM3Dq on one side of hippocampi, and tested whether PET can successfully capture CNO-provoked activations of a neural circuit. Remarkably, sequential PET scans with [^{18}F]FE-TMP demonstrated significant accumulation of [^{18}F]FE-TMP radiosignals at 24 h after injection of CNO (**Figs. 2D and 2E**). A postmortem analysis of brain tissues collected from these mice following PET experiments demonstrated induced expression of ecDHFR-d2Venus primarily in the hippocampal dentate gyrus and CA3 neurons (**Fig. S7B),** and there was good correlation between PET signals and reporter expressions (**Fig. 2E**). These data indicate that [^{18}F]FE-TMP PET successfully captured the chemogenetic activation of the hippocampal network with high sensitivity and specificity.

We next sought to determine whether our imaging techniques can be leveraged to trace neural circuits in deep brain regions of live non-human primates in more detail than rodents. Given the similarity of anatomies of monkey and human brains, we reasoned that this approach could further validate the current method for future medical applications. An AAV encoding ecDHFR-EGFP was delivered to one side of the neocortex and striatum of a 3.4-year-old male common marmoset to express the reporter in the telencephalon. PET scans of this animal with [^{18}F]FE-TMP were performed 45 days after virus injection. To our surprise, the PET scans revealed robust accumulation of [^{18}F]FE-TMP not only in brain regions proximal to the injection site (i. e., neocortex, caudate nucleus, and putamen) but also in other spatially segregated but interconnected areas, including the thalamus and midbrain substantia nigra (**Fig. 3A**). The marmoset brain displayed more efficient radioligand uptake than the mouse brain, and the putamen-to-cerebellum ratio of radioactive signals increased up to 4 at the end of the dynamic PET scan (**Fig. 3B**). Again, distribution of the radioactive signal was consistent with the localization of transgene expression, as assessed by postmortem microscopic imaging of brain sections (**Fig. 3C**). It is accordingly likely that the current ecDHFR-based reporters, particularly in combination with the RAM system, are capable of pursuing chemogenetic activation of a specific neural connection in non-human primates, which has been technically enabled by DREADD and DCZ in our recent work (*11*).

In the final set of experiments, we aimed to explore further applications of unique ecDHFR mutants for PET assays of the protein dynamics in the brain circuit. To this end, we employed an ecDHFR mutant with a destabilized domain (DD) which enabled us to control gene expression and function of a protein of interest (POI) fused to DD in a manner inducible by TMP administration (**Figs. 4A and S8**) (*17, 18*). In agreement with previous studies, treatments with TMP rapidly restored the levels of DD-EGFP in the mouse brain (**Figs. 4B**

and **4C**). We subsequently utilized a cyclic phosphodiesterase, PDE10A, as a POI, which can be detected by PET with a specific radioligand, [^{18}F]MNI659 (*19*). The catalytic domain of human PDE10A (hPDE10A_CD, **Figs. S9A and S9B**) was incorporated in AAVs encoding hPDE10A_CD-EGFP with N-terminal ecDHFR or DD tags and was inoculated into the neocortex. PET scans demonstrated a significant accumulation of [^{18}F]MNI659 in the ipsilateral area expressing DD-hPDE10A_CD-EGFP following peripheral delivery of TMP, suggesting that PET can be used to monitor acute drug-inducible stabilization of DD-POIs in a brain circuit (**Figs. 4D** and **4E**). Hence, the current technology would serve for manipulation of molecular signaling by switching POI on and off and for assessing the functionality of protein degradation systems in healthy and diseased neural networks.

We also relied on a protein-fragment complementation assay (PCA) to clarify the usability of ecDHFR split mutants for monitoring the oligomerization of misfolded microtubule-associated protein tau, which may propagate through the neural network, leading to neurodegeneration in the pathological cascade of Alzheimer's disease (*20, 21*). We constructed an ecDHFR-PCA system in which the N- and C- terminal fragments of the ecDHFR protein (NTF and CTF, respectively) reassemble, thereby restoring its capability to bind to TMP, through interaction between a bait and prey (**Figs. 4F and S10A-S10D**). As a proof-of-principle experiment, TMP-HEX efficiently labeled cultured cells co-expressing NTF and CTF conjugated to a human tau repeat domain (TRD), suggesting that the self-assembly of TRD was spontaneously initiated and could be detected by our method *in vitro* (**Figs. 4G** and **4H**). We therefore co-injected AAVs encoding TRD-NTF and TRD-CTF in the somatosensory cortex, and conducted PET scans with [^{18}F]FE-TMP to detect potential tau oligomerization and propagation *in vivo* more than one month after the surgical procedure. Remarkably, we found an accumulation of [^{18}F]FE-TMP in the proximity of the inoculation site (**Fig. 4H**), and an ipsilateral-to-contralateral ratio of PET signals in a steady state was significantly increased in brains of these mice relative to control brains (**Figs. 4I** and **4J**). A PET scan with [^{11}C]PBB3, a potent PET tracer for fibrillary deposits of pathological tau proteins (*22*), did not reveal any significant accumulation of radioactive signals in the areas receiving the AAV delivery (**Fig. S10E and S10F**). Hence, PET scans with [^{18}F]FE-TMP could capture low-order, PBB3-undetectable tau assemblies, which potentially propagate along a specific brain circuit in the brains of intact animals.

In summary, we have designed and validated new ecDHFR-based reporters and their ligands for complementary fluorescence and PET analyses of the spatial distribution, stability,

and aggregation of genetically-targeted fusion proteins in brain circuits of live animals. Importantly, neither overexpression of the reporter nor repetitive treatment with TMP affects neuronal physiology and animal behaviors (*17, 23*). Accordingly, our approaches enable high-contrast imaging and operations of a specific molecule at a network level in physiological and pathophysiological conditions, which is a task that could not be easily accomplished by conventional techniques. For instance, when driven by cell type-specific or activity-regulated promoters, ecDHFR reporters become instrumental for understanding how various biologically active molecules as represented by optogenetic and chemogenetic tools acutely impact the neural circuit structure and brain function in mice and non-human primates. In genetically engineered animals, our technology allows a longitudinal whole-brain assessment of cell type distribution, brain-wide circuit reorganization, and pharmacological effects on the circuit integrity in living animals. Moreover, ecDHFR-PCA could help to elucidate the mechanisms of neurodegenerative proteinopathies, as Holmes et al. have recently established a fluorescence resonance energy transfer-based assay to monitor the seeding ability of tau aggregates *in vitro* (*24*). In conjunction with currently available imaging modalities such as functional magnetic resonance imaging and functional near-infrared spectroscopy (*25*), our reporter methodologies will facilitate the construction of new assaying systems elucidating links between molecules and functions in a target network. Since the ecDHFR-TMP system is suitable for mammals, recent advances in the design of viral tools for non-invasive gene delivery make it feasible to eventually apply these reporters to biomedical PET imaging of human brains (*26*).

Acknowledgments:

We thank Dr. Atsushi Miyawaki (RIKEN, Saitama, Japan) and Dr. Haruo Kasai (Tokyo University, Tokyo, Japan) for helpful comments on the manuscript. We thank Drs. Tetsuo Yamamori and Masanari Ohtsuka (RIKEN, Saitama, Japan) for sharing a plasmid encoding RAM promoter. We also thank Shoko Uchida, Kaori Yuki, and Katsushi Kumada for technical assistance, and all laboratory members for discussions and encouragement. This study was supported in part by JST CREST Grant Number JPMJCR1652 (M.H.), AMED Grant Number JP19dm0207072 (M.H.) and JP19dm0107146 (T.M.), and JSPS KAKENHI Grant Number 18H04752 (M.S.) and 18K07777 (M.S.).

Author contributions:

M.S. and M.H. conceived the study; M.S. generated expression vectors and recombinant viruses, and performed biochemical and histological analyses; M.S., H.T., M.T., Y.S., Y.T., and N.S. carried out *in vitro* and *in vivo* fluorescence imaging studies; M.O. performed autoradiography and *in vitro* binding assays; J.M, T.M., M.O., and T.K. analyzed TMP metabolites; M.-R.Z. and M.F. supervised chemical design, synthesis, and radioactive probing; M.S., M.T., C.S. and Y.T. performed PET and data analysis; K.M., Y.N., and T.M. performed PET and histological analysis of the primate. M.H, A.M, N.S, T.S. and M.S. wrote the manuscript.

References

1. Z. J. Huang, H. Zeng, Genetic approaches to neural circuits in the mouse. *Annual review of neuroscience* **36**, 183-215 (2013).
2. M. Z. Lin, M. J. Schnitzer, Genetically encoded indicators of neuronal activity. *Nature neuroscience* **19**, 1142-1153 (2016).
3. A. Hayashi-Takagi *et al.*, Labelling and optical erasure of synaptic memory traces in the motor cortex. *Nature* **525**, 333-338 (2015).
4. S. Iwano *et al.*, Single-cell bioluminescence imaging of deep tissue in freely moving animals. *Science* **359**, 935-939 (2018).
5. M. A. Busche *et al.*, Tau impairs neural circuits, dominating amyloid-beta effects, in Alzheimer models in vivo. *Nature neuroscience* **22**, 57-64 (2019).
6. M. Shimojo, M. Higuchi, T. Suhara, N. Sahara, Imaging Multimodalities for Dissecting Alzheimer's Disease: Advanced Technologies of Positron Emission Tomography and Fluorescence Imaging. *Frontiers in neuroscience* **9**, 482 (2015).
7. T. F. Massoud, A. Singh, S. S. Gambhir, Noninvasive molecular neuroimaging using reporter genes: part II, experimental, current, and future applications. *AJNR. American journal of neuroradiology* **29**, 409-418 (2008).
8. T. Haywood *et al.*, Positron emission tomography reporter gene strategy for use in the central nervous system. *Proceedings of the National Academy of Sciences of the United States of America* **116**, 11402-11407 (2019).
9. B. Ji *et al.*, Multimodal Imaging for DREADD-Expressing Neurons in Living Brain and Their Application to Implantation of iPSC-Derived Neural Progenitors. *The Journal of neuroscience : the official journal of the Society for Neuroscience* **36**, 11544-11558 (2016).
10. Y. Nagai *et al.*, PET imaging-guided chemogenetic silencing reveals a critical role of primate rostromedial caudate in reward evaluation. *Nature communications* **7**, 13605 (2016).
11. Y. Nagai *et al.*, Deschloroclozapine: a potent and selective chemogenetic actuator enables rapid neuronal and behavioral modulations in mice and monkeys. *bioRxiv*, 854513 (2019).
12. J. L. Gomez *et al.*, Chemogenetics revealed: DREADD occupancy and activation via converted clozapine. *Science* **357**, 503-507 (2017).

13. C. T. Liu *et al.*, Functional significance of evolving protein sequence in dihydrofolate reductase from bacteria to humans. *Proceedings of the National Academy of Sciences of the United States of America* **110**, 10159-10164 (2013).
14. L. W. Miller, Y. Cai, M. P. Sheetz, V. W. Cornish, In vivo protein labeling with trimethoprim conjugates: a flexible chemical tag. *Nature methods* **2**, 255-257 (2005).
15. M. A. Sellmyer *et al.*, Quantitative PET Reporter Gene Imaging with [11C]Trimethoprim. *Molecular therapy : the journal of the American Society of Gene Therapy* **25**, 120-126 (2017).
16. A. T. Sorensen *et al.*, A robust activity marking system for exploring active neuronal ensembles. *eLife* **5**, (2016).
17. R. Sando, 3rd *et al.*, Inducible control of gene expression with destabilized Cre. *Nature methods* **10**, 1085-1088 (2013).
18. S. Pieraut *et al.*, Experience-dependent remodeling of basket cell networks in the dentate gyrus. *Neuron* **84**, 107-122 (2014).
19. D. S. Russell *et al.*, The phosphodiesterase 10 positron emission tomography tracer, [18F]MNI-659, as a novel biomarker for early Huntington disease. *JAMA neurology* **71**, 1520-1528 (2014).
20. S. S. Shekhawat, I. Ghosh, Split-protein systems: beyond binary protein-protein interactions. *Current opinion in chemical biology* **15**, 789-797 (2011).
21. M. Goedert, M. Masuda-Suzukake, B. Falcon, Like prions: the propagation of aggregated tau and alpha-synuclein in neurodegeneration. *Brain* **140**, 266-278 (2017).
22. M. Maruyama *et al.*, Imaging of tau pathology in a tauopathy mouse model and in Alzheimer patients compared to normal controls. *Neuron* **79**, 1094-1108 (2013).
23. M. Iwamoto, T. Bjorklund, C. Lundberg, D. Kirik, T. J. Wandless, A general chemical method to regulate protein stability in the mammalian central nervous system. *Chemistry & biology* **17**, 981-988 (2010).
24. B. B. Holmes *et al.*, Proteopathic tau seeding predicts tauopathy in vivo. *Proceedings of the National Academy of Sciences of the United States of America* **111**, E4376-4385 (2014).

25. V. Scarapicchia, C. Brown, C. Mayo, J. R. Gawryluk, Functional Magnetic Resonance Imaging and Functional Near-Infrared Spectroscopy: Insights from Combined Recording Studies. *Front Hum Neurosci* **11**, 419 (2017).
26. K. Y. Chan *et al.*, Engineered AAVs for efficient noninvasive gene delivery to the central and peripheral nervous systems. *Nature neuroscience*, (2017).

Figure 1

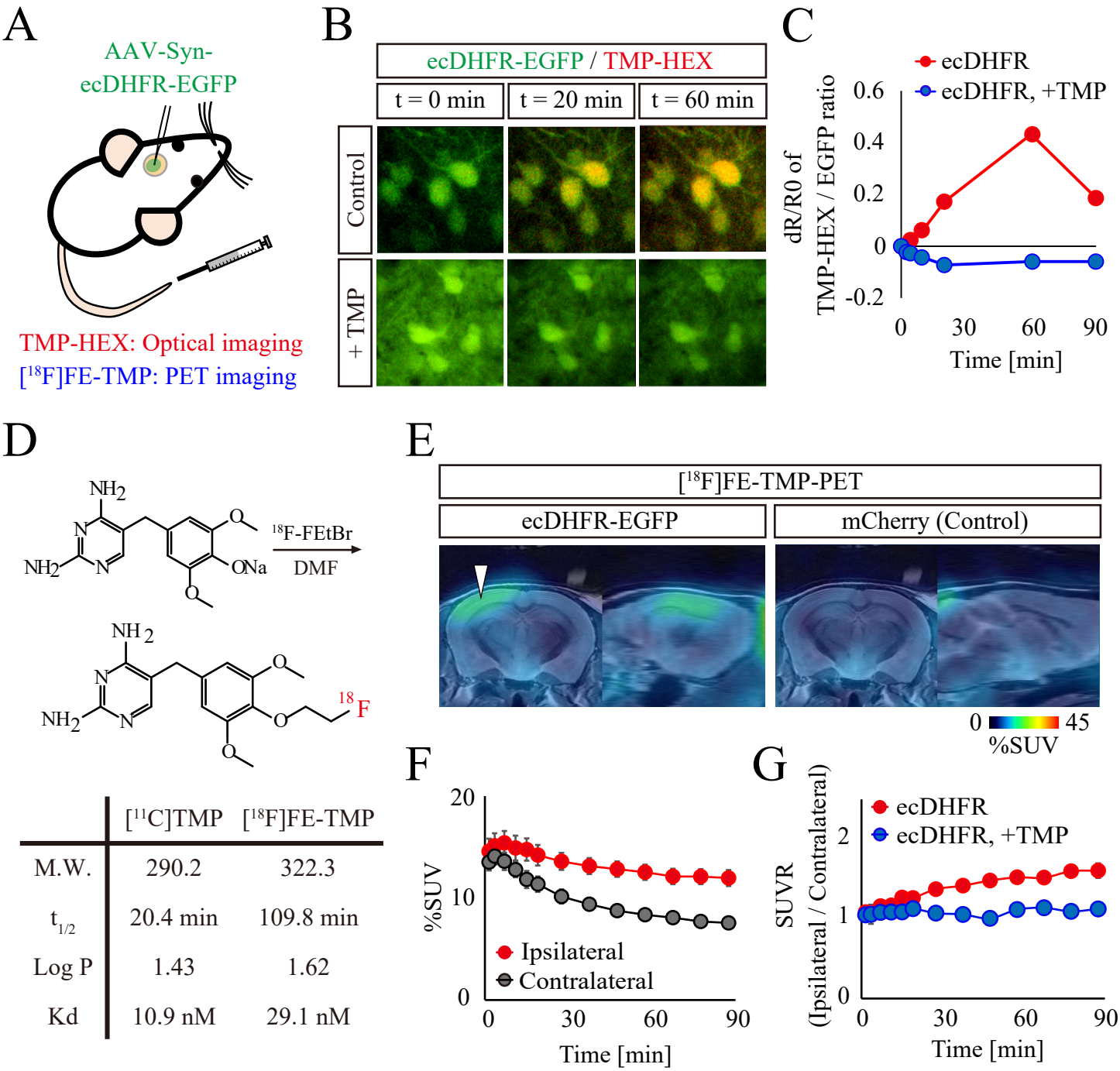

	[11C]TMP	[18F]FE-TMP
M.W.	290.2	322.3
$t_{1/2}$	20.4 min	109.8 min
Log P	1.43	1.62
Kd	10.9 nM	29.1 nM

Figure 1. *In vivo* visualization of ecDHFR with TMP-HEX and [^{18}F]FE-TMP

(**A**) Schematic illustration of bimodal optical and PET reporter imaging in the brain of living mice. Recombinant ecDHFR-EGFP reporter proteins were introduced into the somatosensory cortex with AAV. Two-photon imaging and PET scan were conducted after intravenous administration of TMP analogs, TMP-conjugated fluorescence dye (TMP-HEX), and TMP labeled with radioisotope ([^{18}F]FE-TMP), respectively.

(**B-C**) Peripherally delivered TMP-HEX penetrates the BBB and labels exogenously expressed ecDHFR in the mouse brain *in vivo*. Brains of awake animals were imaged under a two-photon microscope following tail vein administration of TMP-HEX (500 μg/kg).

(**B**) Typical merged images of EGFP (green) and TMP-HEX (red) fluorescence in mice that were given TMP-HEX alone (Control) or together with conventional TMP (i.p., 100 mg/kg). Each image is an average of 10 frames from serial z-stacks.

(**C**) Ratios of TMP-HEX fluorescence intensity relative to EGFP, plotted as a function of time. Averaged values from two independent experiments (20 cells/2 mice for each condition) are shown.

(**D**) Chemical structure and physical parameters of [^{18}F]FE-TMP compared to conventional [^{11}C]TMP.

(**E-G**) AAVs encoding ecDHFR-EGFP or mCherry (as control) were unilaterally injected into the somatosensory cortex. PET scans were performed after peripheral administration of radioactive TMP analog, [^{18}F]FE-TMP alone, or [^{18}F]FE-TMP together with conventional TMP (100 mg/kg).

(**E**) Representative PET images (coronal and sagittal sections) generated by averaging dynamic scan data at 60-90 min after i.v. injection of [^{18}F]FE-TMP. Template MRI images were overlaid for spatial alignment. Arrowhead indicates the areas of accumulation of the radioactive ligand in animals carrying ecDHFR-EGFP (left).

(**F**) [^{18}F]FE-TMP labeling kinetics in the brain of ecDHFR-EGFP-expressing mice (Mean ± SEM, n = 16). $F(1, 30) = 8.753$; $p < 0.01$ (two-way, repeated measure ANOVA). VOIs were manually placed on ipsilateral and contralateral areas for quantification.

(**G**) SUVR (%SUV ratio) of ipsilateral/contralateral signals in the brain of ecDHFR-EGFP-expressing mice after bolus injection of [^{18}F]FE-TMP alone (n = 16) or together with conventional TMP (i.p., 100 mg/kg, n = 4). Data are plotted as Mean ± SEM. $F(1, 18) = 6.896$; $p < 0.05$ (two-way, repeated measure ANOVA).

Figure 2

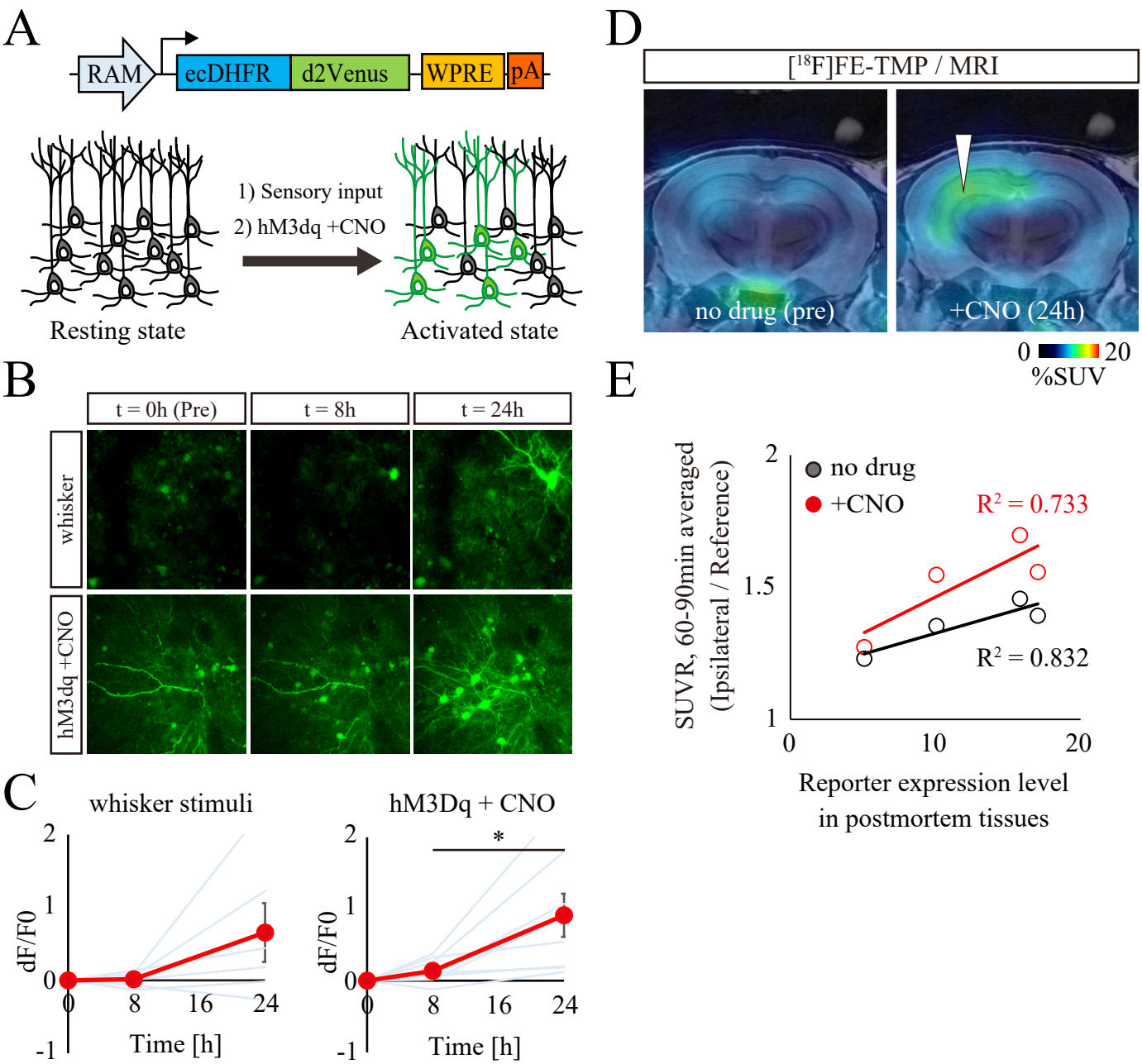
A
RAM
ecDHFR
d2Venus
WPRE
pA
1) Sensory input
2) hM3dq +CNO
Resting state
Activated state
B
t = 0h (Pre)
t = 8h
t = 24h
whisker
hM3dq +CNO
C
whisker stimuli
hM3Dq + CNO
dF/F0
Time [h]
D
[18F]FE-TMP / MRI
no drug (pre)
+CNO (24h)
0
20
%SUV
E
SUVR, 60-90min averaged (Ipsilateral / Reference)
no drug
+CNO
R2 = 0.733
R2 = 0.832
Reporter expression level in postmortem tissues

Figure 2. *In vivo* visualization of neuronal ensemble activation in response to sensory stimuli and hM3Dq-DREADD

(**A**) Schematic illustration of virus construction and marking of neuronal ensemble activation by CNO mediated hM3Dq-DREADD activation.

(**B** and **C**) AAVs encoding ecDHFR fused to destabilized Venus (ecDHFR-d2Venus) with RAM promoter and hM3Dq were co-introduced into two segregated regions of the somatosensory cortex and imaged under two-photon microscope.

(**B**) Fluorescent intensity of ecDHFR-d2Venus in the brain of awake animals was analyzed before (0 min) and after (8 h or 24 h) air-puff mediated whisker stimulation (10 sec, 5 times) or chemogenetic activation of hM3Dq via peripheral administration of CNO (10 mg/kg). Averaged images of 10 stacked frames in serial z position are shown.

(**C**) Averaged ecDHFR-d2Venus fluorescence intensities, plotted as dF/F0 ratios at different time points after neuronal activation. Data from 6-8 regions / 3-4 mice for each condition are plotted as Mean ± SD (red line) and individual regions (blue line). 8 h vs 24 h, $F(2, 21) = 7.715$; $*p < 0.05$ (one-way ANOVA).

(**D-E**) Mice expressing ecDHFR-d2Venus and hM3Dq in a side of hippocampus was sequentially analyzed by [^{18}F]FE-TMP PET imaging before (left) or 24 h after (right) intraperitoneal CNO injection (0.3 mg/kg).

(**D**) Representative PET images demonstrate that 0.3 mg/kg CNO-mediated activation of hM3Dq enhanced the accumulation of radioactive signals in the hippocampus. Averaged images of dynamic scan data at 60-90 min after i.v. injection of [^{18}F]FE-TMP are shown. Template MRI images were overlaid for spatial alignment. Arrowhead indicates selective accumulation of radioactive signals in the AAV injection site after CNO administration.

(**E**) SUVR (%SUV ratio) of ipsilateral hippocampi / reference region (brain stem) signals during dynamic PET scans. Data from ecDHFR-d2Venus expressing mice (n = 4) before and after 0.3 mg/kg CNO i.p. injection are plotted. Correlation with R^2 values between SUVR of [^{18}F]FE-TMP_PET and expression levels of ecDHFR-d2Venus (fluorescence) in postmortem tissues was determined by linear regression analysis.

Figure 3

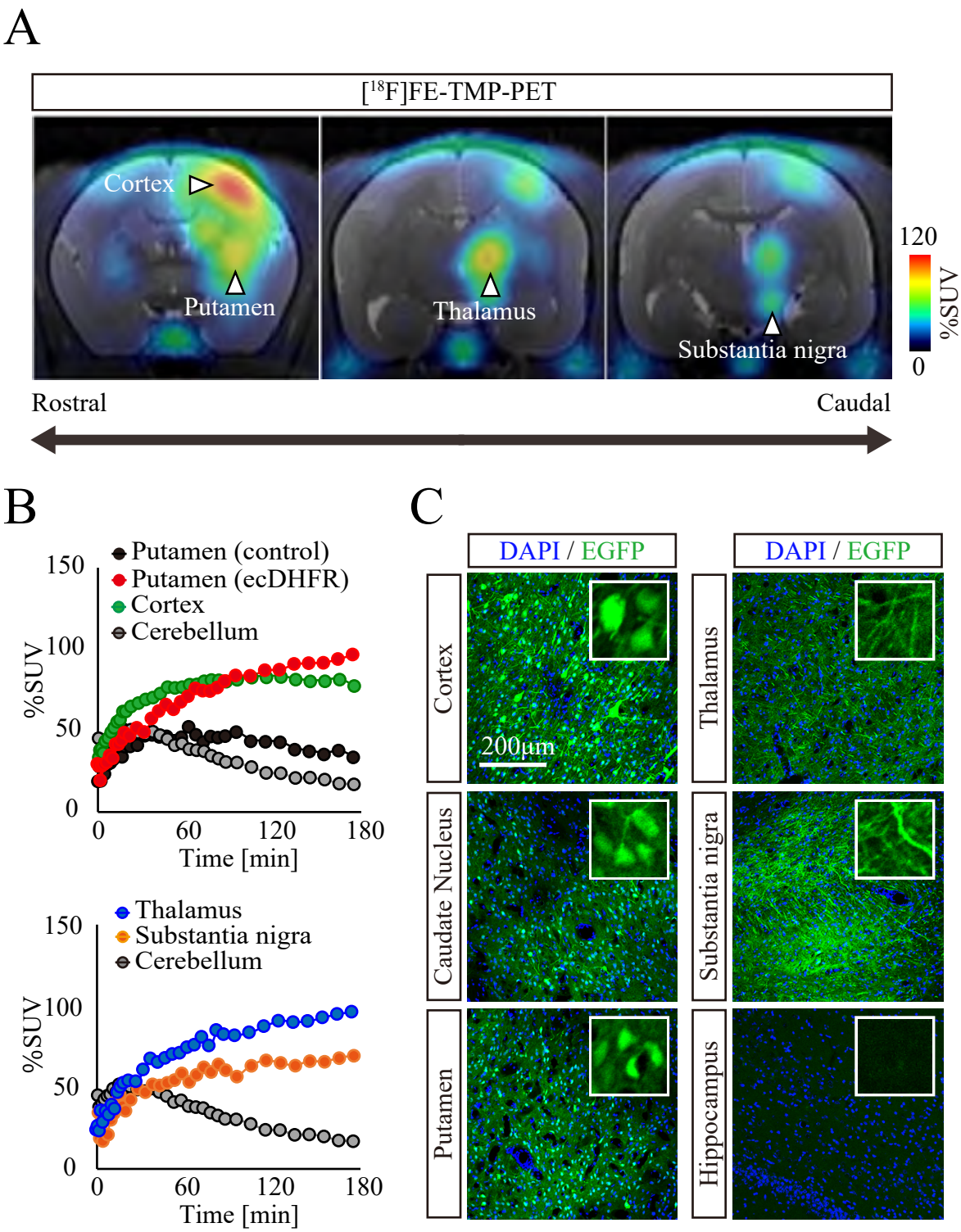
A
[18F]FE-TMP-PET
Cortex
Putamen
Thalamus
Substantia nigra
120
%SUV
0
Rostral
Caudal
B
Putamen (control)
Putamen (ecDHFR)
Cortex
Cerebellum
150
100
50
0
%SUV
0
60
120
180
Time [min]
Thalamus
Substantia nigra
Cerebellum
150
100
50
0
%SUV
0
60
120
180
Time [min]
C
DAPI / EGFP
DAPI / EGFP
Cortex
Thalamus
200μm
Caudate Nucleus
Substantia nigra
Putamen
Hippocampus

Figure 3. PET imaging of ecDHFR/TMP reporters in primate brain

ecDHFR-EGFP was expressed in the brain of a 3.4-year-old common marmoset with an AAV. PET scans of [^{18}F]FE-TMP were performed 45 days after virus injection.

(**A**) Representative coronal PET images generated by averaging dynamic scan data at 60 - 180 min after i.v. injection of [^{18}F]FE-TMP (left). Note that reporter molecule was densely distributed in thalamus and substantia nigra pars compacta, which are connected to the neocortex and putamen via direct neuronal tract, respectively. PET images are overlaid with an MRI template. Scale bar represents %SUV.

(**B**) Time-radioactivity curves for [^{18}F]FE-TMP in the putamen carrying ecDHFR-EGFP (red symbols) or control AAV (black symbols), neocortex (green symbols), and cerebellum (filled gray symbols) are displayed in the upper panel. Curves in the thalamus (blue symbols) and substantia nigra (orange symbols) along with cerebellar data are also shown in the lower panel.

(**C**) Postmortem analysis of ecDHFR-EGFP expression in brain slices. Representative images illustrate EGFP fluorescence in the cortex, caudate nucleus, putamen, thalamus, and substantia nigra. High magnification image frames are shown in inserts.

Figure 4

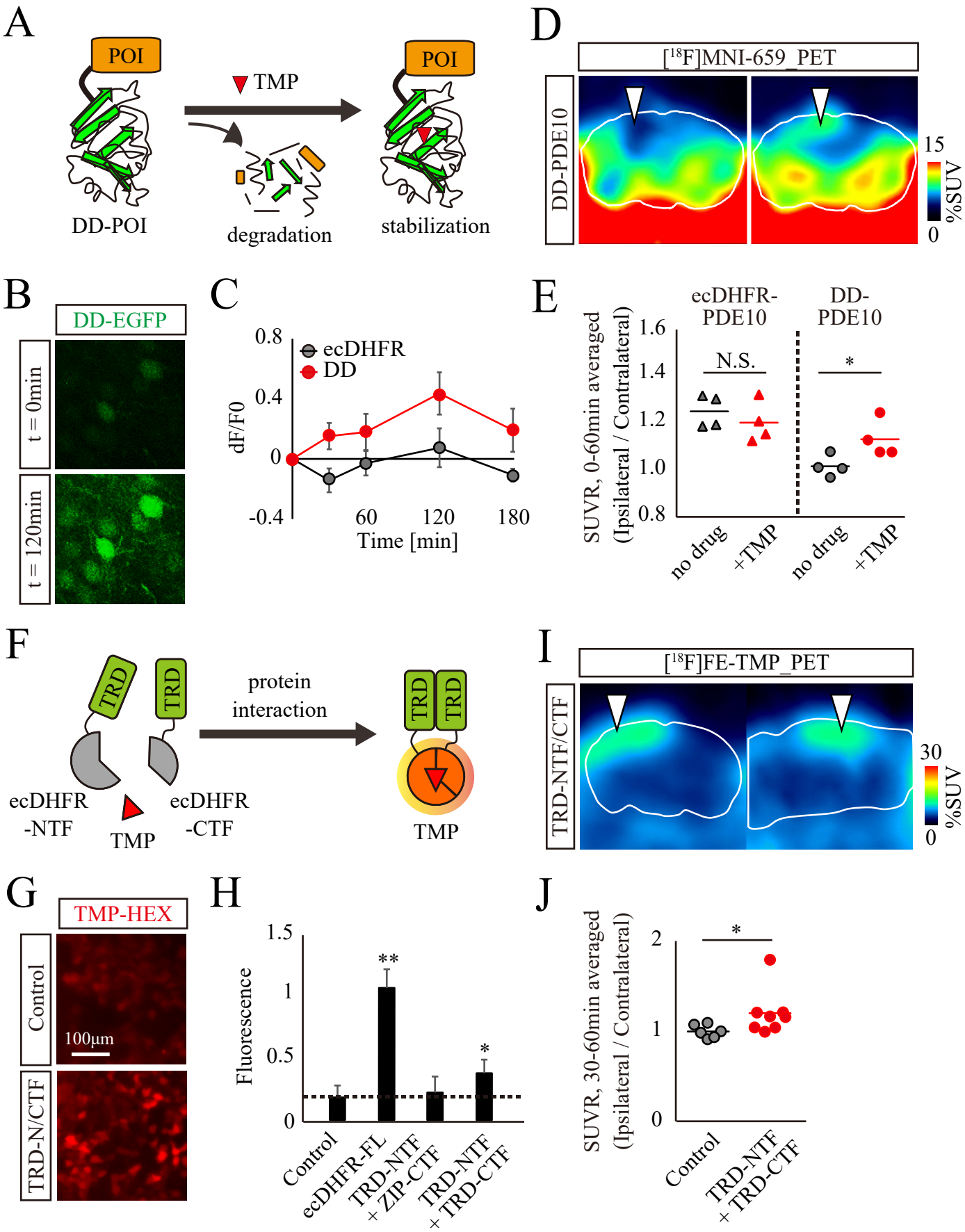
A
POI
TMP
POI
DD-POI
degradation
stabilization
D
[18F]MNI-659_PET
DD-PDE10
15
%SUV
0
B
DD-EGFP
t = 0min
t = 120min
C
0.8
0.4
0
-0.4
ecDHFR
DD
dF/F0
60
120
180
Time [min]
E
ecDHFR-PDE10
DD-PDE10
N.S.
*
SUVR, 0-60min averaged (Ipsilateral / Contralateral)
1.6
1.4
1.2
1.0
0.8
no drug
+TMP
no drug
+TMP
F
TRD
TRD
protein interaction
TRD
TRD
ecDHFR -NTF
TMP
ecDHFR -CTF
TMP
I
[18F]FE-TMP_PET
TRD-NTF/CTF
30
%SUV
0
G
TMP-HEX
Control
100μm
TRD-N/CTF
H
1.5
1
0.5
0
Fluorescence
**
*
Control
ecDHFR-FL
TRD-NTF + ZIP-CTF
TRD-NTF + TRD-CTF
J
SUVR, 30-60min averaged (Ipsilateral / Contralateral)
2
1
0
*
Control
TRD-NTF + TRD-CTF

Figure 4. PET analysis of TMP-inducible protein stabilization and protein-protein interaction in the brain

(**A**) Schematic illustration of TMP-dependent control of DD-POI protein turnover. A protein of interest (POI) fused to a destabilizing domain (DD) undergoes rapid degradation by ubiquitin-proteasome system, while POI can be stabilized in the presence of TMP.

(**B** and **C**) Mice expressing fusion proteins comprised of EGFP and either wild-type or destabilized mutant ecDHFR (ecDHFR-EGFP or DD-EGFP, respectively) were imaged by two-photon microscope. The constructs were introduced into the somatosensory cortex with AAVs.

(**B**) Fluorescent intensity of DD-EGFP in intact brains of awake animals was analyzed before (0 min) and after (120 min) peripheral administration of TMP (100 mg/kg). Averaged images of 10 stacked frames in serial z position are shown.

(**C**) Averaged ecDHFR-EGFP and DD-EGFP fluorescence intensities plotted as dF/F0 ratios at different time points after TMP delivery. Data from 10 neurons for each genotype are plotted as Mean ± SD.

(**D-E**) ecDHFR-PDE10 and DD-PDE10 were expressed in a caudal region of cortical hemisphere from an AAV. Accumulation of the radioactive signal was monitored by PET scan with [^{18}F]MNI659, a selective radioactive PET ligand against PDE10.

(**D**) Representative PET images demonstrate the detection of TMP-stabilized DD-PDE10 in caudal area of the neocortex. Averaged images of dynamic scan data at 0-30 min after i.v. injection of [^{18}F]MNI659 are shown. 90-min scans were conducted before or 2 h after intraperitoneal TMP injection (100 mg/kg). White lines mark the whole brain area as determined by MRI. Note selective accumulation of radioactive signals in the AAV injection site by TMP administration (arrowheads).

(**E**) Averaged SUVR (%SUV ratio) of ipsilateral/contralateral radioactive signals during 0-60 min scan in individual animals expressing ecDHFR-PDE10 (n = 4) or DD-PDE10 (n = 4). Data represent Mean (horizontal bar) and values from individual animals (dots) for each group under control condition (no drug) or after TMP treatment. *$p < 0.05$ (Student's t-test). Note a significant TMP-dependent increase of the ratio in animals carrying a destabilized reporter.

(**F**) Schematic representation of a reporter containing the N- and C-terminal ecDHFR fragments (NTF and CTF). These fragments reassemble after interaction of fused proteins A and B, thereby restoring the TMP-binding ability.

(**G**) Representative images illustrate a selective retention of TMP-HEX in cells expressing ecDHFR NTF and CTF fused with human tau repeat domain (TRD).

(**H**) TRD oligomerization-dependent TMP-HEX labeling was quantitatively analyzed in cells expressing various combinations of ecDHFR-NTF and CTF fragments as normalized fluorescence intensities. Mean value of full-length ecDHFR (ecDHFR-FL) was set as 1. Data from seven independent experiments are shown as Mean ± SD. $F(3, 24) = 77.86$; $^{**}p < 0.01$, $^{*}p < 0.05$ (one-way ANOVA followed by Dunnett post-hoc test).

(**I-J**) PET analysis of Tau oligomerization in the brain. 90-min [^{18}F]FE-TMP PET scans were conducted after co-injection of AAVs encoding TRD-NTF and TRD-CTF into one hemisphere of the somatosensory cortex.

(**I**) Representative PET images (coronal and sagittal sections from left) were generated by averaging dynamic scan data at 60-90 min after i.v. injection of [^{18}F]FE-TMP. Images show a selective accumulation of radioactive signals in the AAV injection site (arrowheads). White lines mark the whole brain area as determined by template MR image.

(**J**) Averaged SUVR (%SUV ratio) of ipsilateral/contralateral radioactive signals during 15-60 min dynamic PET scans. Data from Control mice ($n = 6$; mixture of uninfected mice, $n = 4$ and TRD-NTF/ZIP-CTF-expressing mice, $n = 2$) or TRD-NTF/TRD-CTF-expressing mice ($n = 8$) are plotted as Mean (horizontal bar) and individual animals (dots). $^{*}p < 0.05$ (Mann-Whitney test)